3D effects in microwave radiative transport inside precipitating clouds: Modeling and applications

Chapter 1

3D EFFECTS IN MICROWAVE RADIATIVE TRANSPORT INSIDE PRECIPITATING CLOUDS: MODELING AND APPLICATIONS

Alessandro Battaglia,[1] Franco Prodi,[2], Federico Porcú[1] and Dong-Bin Shin[3]

[1] *University of Ferrara, via Paradiso 12, Ferrara, Italy*
batta@fe.infn.it

[2] *ISAC-CNR, via Gobetti, Bologna, Italy*

[3] *School of Computational Sciences,George Mason University, Fairfax, Virginia*

Abstract New rainfall tecniques urge microwave physically based retrievals to produce an estimate error, to be more precise at the istantaneous level and to provide a correct geolocation of the raining areas. Within 3D structured clouds the coupling between horizontal and vertical disomogeneity introduces additional uncertainties to instantaneous estimate because of the azimuthal dependence of the radiation field. In fact conical scanning microwave radiometers looking at the same point at the ground from different positions may measure quite different brightness temperatures. For radiometric scene over specular surfaces, this 3D radiative effect, avaraged over TMI-like footprint, can be fully described by 1D slant path models, except for strongly scattering highly developed raining cells at 85 GHz.

A simulation radiative transfer study applied to Goddard Cumulus Ensemble Cloud Resolving Models, shows that the fore/after view configuration, now available for some new generation sensors, may help in capturing features like tilted or different stage raining cells, emission peaks, asymmetric ice decks, ..., especially in convective regions. This definitely leads to a better insight in the slant path cloud properties and to an improvement of Bayesan technique driven rain retrievals.

Keywords: microwave radiative transfer, 3D effects, slant path

1. Introduction

Microwave radiative transfer computations are increasing their relevance as the emphasis in rainfall "physically" based satellite remote sensing retrievals ([15] and reference therein) increases. In fact, these approaches use statistical methods to match observed T_Bs with an appropriate T_Bs database, pre-computed by forward radiative transfer (RT, hereafter) computations applied to a properly selected datasets of atmospheric profiles. In this sense the word "physically" implies the attempt to model the dynamic, the microphysics and the radiative properties of the precipitating system under observation. This approach is double-edged: its strength resides in the possibility of evaluating how each single effects impacts the non linear $T_B - RR$ relationship and, thus of tempting an error estimate of the RR product; conversely its weakness resides in the chance that one of this complex modeling can be badly described, thus spoiling all the retrieval.

Until recently the major part of MW rainfall products has been intended for climatological purposes; at this level temporal and spatial averaging washes out many uncertainties typical of the retrieval procedure, primarily all these effects connected to the 3D structure of clouds. To our knowledge all rain retrieval algorithms from multi-spectral microwave measurements have presumed the existence of plane parallel clouds, that allows fast RT forward computations. Only in a second moment many authors have investigated biases and random errors which are introduced when an inherently 3D problem is treated with a 1D solution ([8]), but the most attention has been paid to 3D effects that induces a bias in the retrieval (the beam filling effect overall). In view of the next generation available sensor packages (MSG and those following in the GPM concept overall), a renewed impulse to instantaneous rainfall estimates has been done by blending techniques where quantitative MW algorithms train the geo-stationary rapid update cycle. In fact, over ocean (where we concentrate our analysis), thanks to their slicing capabilities,multi-spectral passive microwave techniques perform superiorly for instantaneous applications respect to VIS/IR techniques which generally infer precipitation only from cloud top information. While for temporally accumulated product large temporal sampling errors overcome spatial sampling effects, at the instantaneous level the coarse spatial resolution of PMW sensors is a critical issue. Therefore in order to achieve a real improvement in a correct location of the raining pixels ([2]), in the discrimination rain/no rain, and in the estimate of the rain rate with a physically based error (bias+root mean square error), the interplay between the characteristics of the PMW observing system (like

spatial resolution, viewing geometry, instrument frequency and polarization) and of the observed cloud system (actual geometry of the cloud, that is vertical and horizontal development and patch structures, vertical and horizontal in-homogeneity of scattering parameters) has to be deepened.

In this chapter, after briefly reviewing the state of the art of some well assessed 3D issues, we will focus our attention on some other important 3D effects; in particular we will try to assess when, for a conical scanning radiometer, a $3D$ description is really necessary and which kind of radiative transfer approaches are best suited for different cases. Finally, as a step toward a better understanding of the 3D structure of clouds, we try to investigate and exploit the potentialities of the fore/after viewing radiometer configuration (already realized in Windsat and planned for EGPM radiometers).

2. 3D cloud structure: observations and modeling

The cloud structure inhomogeneity readily observed by in situ and remote measurements (e.g. reflectance imagery, radar profiles) plays a key role in the evaluation of 3D effects in cloud analysis and precipitation retrieval. Convective systems usually presents small scale variability of the horizontal structure, which extends in vertical for several kilometers: studies over tropical regions show that only 5% of the convective updrafts has diameter larger than 4.3 km ([6]), which is the smaller footprint available for passive microwave spaceborne sensors (TMI). Other studies found that the median convective cell size for summer storms near the mid-Atlantic coast of the United States is only 1.9 km [3]. Moreover, for convective mesoscale-organized systems the horizontal asymmetry of the structure is also impacting the represenativeness of a slant path view. Cloud systems as squall lines of the leading-line/trailing- stratiform type, common over the tropics and at mid-latitude as well, has a leading line of contiguous convective cells, separated at scale of the cell size order, and a trailing stratiform cloud shield extending backwards of the leading line.The slant path observation of this kind of systems strongly depends of the viewing direction, and, since they can extend for few hundred kilometers, different parts of the system can be seen with different azimutal angles.

Usually stratified precipitating systems show a more symmetric and shallow 2D structure, that should be less sensitive to slant path observation. The precipitation structure in a typical mid-latitude frontal system, shows different small scale, elongated features (rain bands) of

enhanced precipitation, embedded in the general frontal stratified precipitation pattern. Even deep convection can develop within stratified structures, especially if forced by orography, breaking the horizontal homogeneity at a spatial scale related to the topographic features. In these cases a spatial horizontal gradient of 12 hours cumulated precipitation reaches 120 mm km^{-1} [13]. Slant path observation of dishomogeneous cloud system over complex terrain is even more difficult, given the variability of the orientation and emissivity of the backgroung surface.

Cloud resolving models have given great strides in generating fine-scale cloud and storm properties by providing vertical structure of the atmosphere and of the hydrometeors. Their role is therefore crucial in the modellization of the non linear relationship between hydrometeor concentration and surface RR and in the computation of scattering parameters that are needed to simulate the upwelling T_Bs. Here in the following, as test examples, we use some simulations from the Goddard Cumulus Ensemble Model ([14]), of a tropical squall line and of two midatlantic fronts (warm and cold). At the state, their resolution (2 km or 4 km in the horizontal and 0.5 km in the vertical) is the highest scale at which we can evaluate $3D$ radiative effects.

3. RT computations

Many authors faced the problem of 3D RT computations for raining scenes: Roberti et al., 1994 reviewed and provided a clear intercomparison between different techniques. Compared to other ones (e.g. the VDOM, [4]), the Monte Carlo methods, in its different versions (backward [11]; forward-backward [9]; forward [12], [1]), seems the more suitable to investigate MW RT through complicated 3D structures. In exchange for the simplicity, a fairly substantial computational penalty (reducible with biasing techniques, see [12]) is paid, but certainly manageable for off-line applications. However, in many cases the 3D structure of clouds does not preclude the use of 1D radiative transfer approaches. In fact the plane parallel assumption does not require homogeneity at distances arbitrarily far from the FOV of the sensing instrument ([10]). For instance for pure absorbing atmosphere and Fresnel-like surfaces, the radiation sensed by PMW radiometers originates just in the FOV projected slant tube. In these cases 1D approximations work very well, with the simple expedient of taking in account geometric effects in case of off-nadir looking radiometers ([9]).

In presence of scattering and/or diffusive surfaces, radiation sensed at the satellite may not be originated in the slant tube of observation. In this case it occurs an horizontal displacement of radiation in the direction

perpendicular to the viewing direction; this horizontal displacement can then be used to assess the scales over which horizontal inhomogeneities are important in remote sensing problems. Thanks to its intrinsic tracing procedure, the Monte Carlo techniques makes it possible to record the statistics about the number of scattering events undergone by radiation, the source of the signal (thus the evaluation of the weighting functions), the fraction of radiation coming from outside the observing slant FOV, etc .... This motivates why MC methods are believed to be the most adaptive tool to investigate 3D MW RT aspects.

In the following analysis we will adopt three different RT solutions: a backward Montecarlo, slightly modified from Roberti's code, and the Eddington approximation ([7]) in its 1D plane parallel (PP) and slant path (SP) version (similarly to that already done by [2], [12], [9]). In these two approximations the structure is horizontally homogeneous while the vertical profile is reconstructed by using the vertical profile above the observation point at the ground for the PP, and the slant profile defined by the ray traced from the sensors downward to the surface and then specularly reflected upward for the SP. Note that all calculated T_Bs are ascribed to the position at the ground the sensors is looking at.

4. 3D effects at microwave regime

The T_Bs sensed by PMW sensors are the result of the interplay between the intrinsic 3D structure of the clouds and the radiometer properties. Many different aspects of this interconnection are usually intended as 3D issues. For instance the mismatching between the coarse instrument FOV and the fine-structured cloud horizontal in-homogeneities leads to the *beam filling problem*. In case the radiometer FOV is not uniformly filled, the non-linearity between retrieved physical parameters (like RR, SST, LWC, IWC) and measured T_Bs introduces both bias (for instance an underestimation of the RR in case of rainfall homogeneous assumption across the FOV) and random errors. The way for correcting and estimating these errors has been faced by many authors and can be tackled in different ways ([8] and reference therein).

Here in the following we avoid the beam filling complication (by assuming that the coverage of the rain column within the FOV is known from some other independent measurements) and, by focusing at RT calculations performed at the maximum available resolution (in our case the resolution of the CRM, $2 \times 2\ km^2$ or $4 \times 4\ km^2$), we single out those 3D radiative effects that are not reproducible with 1D approximations. We will briefly categorize them as geometric and diffusion effects.

Geometric effects

At emission channels, upwelling radiation measured by PM radiometers with conical scan geometry (viewing angle Θ_v) results from absorption/emission processes along the whole slant beam. Therefore at low frequency channels the 3D RT problem reduces to a 2-D one. As shown in literature ([16], [9], [11], [2]) leakages coming directly from the warm side of the cloud or scattered by the Fresnel-like cold surface can be accounted for by 1D SP approximation but not by 1D PP modeling[1]. For a fore looking radiometer observing a cloud system with height H_c the geometric effects broaden the radiometric signal of the cloud in a wider region $2H_c \tan\Theta_v$ before and $H_c \tan\Theta_v$ after the physical boundaries of the cloud.

Diffusion effects

At scattering channels, due to the re-directioning of radiation by diffusion events, the measured signal can originate from outside the geometrical slant beam, so that at this level the radiometer is receiving "photons" from a 3D region of the cloud, less defined than the 2-D slant tube.

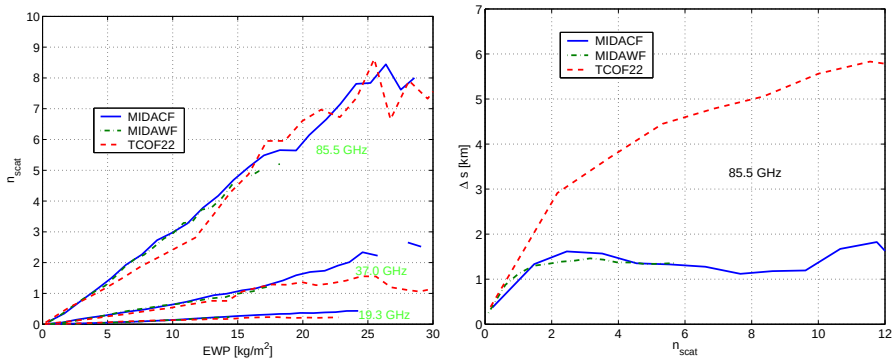

Figure 1.1. Average number of scattering events at three frequencies for different values of the EWP (left panel) and mean lateral displacement Δs vs. average number of scattering at $85.5_H\ GHz$.

To exemplify, we show in fig. 1.1, for the three different CRM simulations, the average number of scattering events (computed with the

[1]Small differences still remain because the intersection between the 3D cloud structure with the slant beam does not result in homogeneous plane parallel layers: in fact the SP approximation does not perfectly accommodate cloud edges!

MC code at TMI footprint) as a function of the slant EWP (equivalent water path) that is the sum of the LWP and the IWP. The number of scattering events increases with the EWP and with the frequency (at 19.3 GHz the scattering becomes negligible) but it is almost independent from the cloud system under observation.

To assess the importance of the $3D$-diffusion effect we have computed $\Delta s_\perp$, the absolute horizontal displacement of radiation in the direction perpendicular to the viewing direction between the emission and the sensor position. In the right panel of fig. 1.1 this quantity is shown as a function of the number of scattering events. In this case the relation strongly depends on the cloud system. For the same number of scattering events (thus the same EWP), the TCOF22, that simulates a squall line system with a very high spatial variability of scattering properties nearby the convective raining cells, have a much greater $\Delta s_\perp$ than the cold and warm front case studies. In fact these two last raining systems do have a lower vertical development (freezing level height is nearly half the value of the squall line) and therefore with the same slant EWP they have a much higher hydrometeor content, hence larger extinction coefficients; this does not allow radiation to travel as much as for the squall line. Note that when the $\Delta s_\perp$ becomes comparable with the horizontal resolution of the radiometer the $3D$ diffusion effects starts being relevant and the $SP-1D$ being quite bad an approximation. For $TMI-$like radiometers, for the simulations of our database, this is true only at the 85.5 GHz.

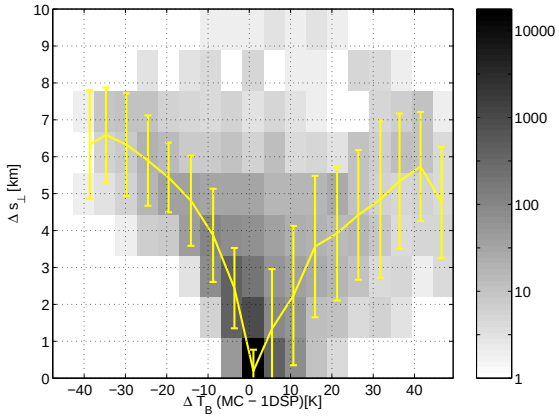

Figure 1.2. Average $\Delta s_\perp$ as a function of the ΔT_B computed between MC and 1D SP approximation at TMI resolution for the H-85.5 GHz. The underlying gray image gives the probability density for these two variables for the analyzed database.

As already noticed by Kummerow ([8]) and consistently with earlier findings in [11], the 1D modeling, compared to the 3D correct one, intro-

duce a rms more then a bias error. In fact in 1D model approximations, radiation remains trapped by construction in the slant tube: no contribution from outside the tube is allowed and abrupt not physical variations may happen for contiguous pixels. 3D MC radiation field can be considered a sort of redistribution of the 1D radiation pattern. The computed $\Delta T_B = T_B(MC) - T_B(1D - SP)$ shows consistent differences ($> 10\,K$) at TMI-like resolution only at the highest frequency (85.5 GHz). Areas with positive ΔT_B are closely followed by areas with negative ΔT_B, thus confirming the redistribution conjecture. Fig. 1.2 shows the difference ΔT_Bs for the whole database at 85.5 GHz, and its strict correlation to the $\Delta s_\perp$. Obviously the presence of consistent $\Delta s_\perp$ (comparable with the instrument FOV) has to couple with an horizontal in-homogeneity of scattering properties to give appreciable differences between 1D and 3D models. Otherwise if these two conditions are not simultaneously satisfied (for instance in an homogeneous thick ice deck or in presence of a strong absorbing inhomogeneous water vapor field) no real 3D effects are really detectable. As a prospective for better instantaneous RR retrievals, the 1D-SP (not the 1D-PP) model partially accommodates for the geometrical problems due to surface scattering and oblique viewing angle but still cannot take into account diffusion effects due to cloud scattering. Therefore it reproduces T_B quite accurately for emission dominated frequencies (10 and 19 GHz, even at CRM resolution) but not at higher frequencies. If convolved to TMI resolution the result remain acceptable for 37.0 GHz but not at 85.5 GHz. Therefore this last frequency (and, a fortiori, higher MW frequencies) has to be treated more carefully by performing dedicated 3D RT simulations especially with high EWP and in coincidence with highly vertically developed and strongly horizontally inhomogeneous raining systems.

5. Fore/after radiometer

From above considerations, we can deduce that TMI-like radiometers sense primarily the 2D slant-tube structure of the cloud. Recently launched (U.S. Navy Coriolis) and future planned spacecrafts (EGPM drone) host or are going to host conically-equipped space-borne MW radiometers able to provide fore/after views of the swath, a novelty respect to imagers like SSM/I and TMI. In this configuration, after a revisitation time of about 5 minutes (for typical LEO satellite), the radiometer is potentially looking at the same[2] scene from the back instead of from

[2]It can assumed that the potential precipitating systems under observation have not significantly changed during the revisitation time, at least over current PMW resolution.

the rear side. Besides well established benefits[3], it has to be evaluated whether or not the use of additional information from backward direction (hence a double number of $T_B s$) can improve the current MW algorithm in term of rain-no rain discrimination, geo-location of raining pixels (like in [2]), retrieval of rain intensity and hydrometeor profile. This goal is here pursued by a simulation study with fore-after T_Bs computed from the former CRM database on a TMI-like radiometer.

Because of different optical paths in $3D-$structured clouds, different $T_B s$ are measured when observing the same pixel at the ground from supplementary directions as shown in fig. 1.3. This allow to reveal fea-

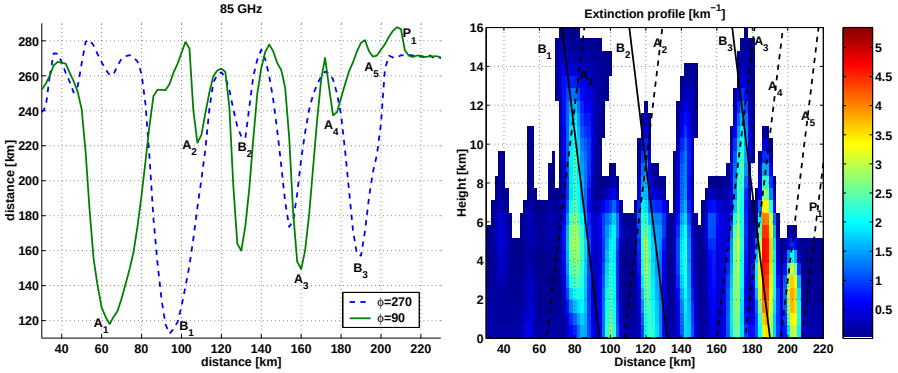

Figure 1.3. Cross section for the extinction coefficient and the simulated fore/after T_B profiles at $85.5_H\ GHz$.

tures and information that cannot be picked up by using one view only. For instance, in fig. 1.3, the comparative study of fore and after minima patterns reveals that, sometimes, fore minima (labeled by B_i) are followed by an after minima (labeled by A_i) with the same cold temperature. The horizontal distance between correspondent minima, through geometric considerations, can be used to a stereographic reconstruction of the altitude of the high concentration ice area causing the T_B depression. [i.e. around 11 km and 9 km for minima (A_1, B_1) and (A_2, B_2) 30 and 24 km horizontally separated respectively]. Other times, due to occultation of emission or scattering areas by close different altitude clouds or tilted systems ([5]), different pattern in the structure of fore/after T_Bs are found. In fig. 1.3 while the fore radiometer detects only one minimum (B_3) the after radiometer detects three minima (A_3, A_4 and A_5).

[3]Primarily the potential to reduce radiometric noise (particularly relevant for polarimetry) by a factor $\sqrt{2}$ through re-mapping to a common grid and averaging, and to check the consistency of the wind retrievals.

This indicates the presence of three side by side convective cells, characterised by different altitude. The first cell (located around $y = 175\ km$) develops higher in the troposphere and obscures the other two, when seen by a forward radiometer. Similarly the side emission peak, originated by very warm emission from the side of the cloud, whether present in one view is not present in the other (in fig. 1.3 P_1 has no correspective maximum).

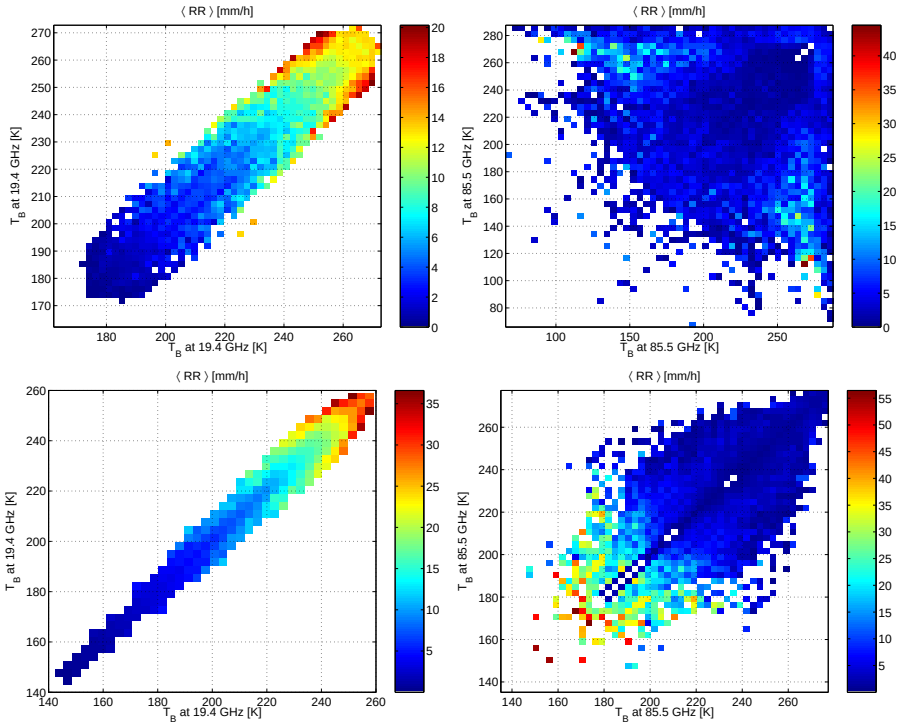

Figure 1.4. Mean RR in the fore/after T_B plane at $19.3_H\ GHz$ (left panels) and $85.5_H\ GHz$ (right panels). Top (bottom) panels correspond to the GCE $TCOF22$ ($MIDACF$) simulation.

A systematic analyses of the simulated fore/afterT_B database shows that the differences in T_Bs are higher and spread out more around the convective cells for higher frequencies (in fig. 1.4 compare right with left panels) and for taller systems (compare top with bottom panels); the higher the RR and the frequency the lower the correlation between fore/after $T_B s$. T_Bs have been grouped in classes $2\,K$-wide and for each pixel mean rain rate $\langle RR \rangle$ and standard deviation $\sigma(RR)$ have been computed for the different TMI-frequency. The error structure for the

fore/after view is substantially better than the error structure of a pure fore configuration, especially at high frequency. To have a very rough index of the improvement that the fore/after configuration could provide versus the single and double looking TMI-radiometer, the total *std* for the RR is computed for each simulation and is shown in Tab.1.1. At

Table 1.1. Quantification of the total stde for the RR computed for different TMI frequency. Here we consider horizontally polarized channel because they are more sensitive due to the lower surface emissivity.

$freq\ [GHz]$	$\sigma(RR)\{1//2T_B\}[mm/hr]$		
	$TCOF22$	$MIDACF$	$MIDAWF$
$10.7_H(1//2T_B)$	0.35//0.35	0.38//0.37	0.22/0.22
$19.3_H(1//2T_B)$	0.82//0.73	0.85//0.81	0.27//0.27
$37.0_H(1//2T_B)$	2.20//1.25	3.21//2.22	0.62/0.44
$85.5_H(1//2T_B)$	4.3//3.3	5.04//3.65	1.99//0.87

10 GHz the fore/after configuration adds practically no information, while the improvement seems to increase at higher frequencies. Note that at 19 and 37 GHz, the two channels more correlated to RR, the best results of the double viewing are obtained for the TCOF22 system.

Retrieval results

To evaluate whether the observations at two different viewing angles really improve the performance of rainfall estimation we have performed synthetic retrievals based on a simple Bayesian approach ([15]). Fig. 1.5 shows the scatter plots of the true and retrieved rain rates for the three different CRM simulations and the two TMI-like radiometers. The first radiometer is assumed to have only a forward view ($\phi = 90°$) and the other one have double views (forward and backward, $\phi = 90° + 270°$). Rain retrieval statistics such as rain bias, RMS statistics and correlation are also represented for each experiment. A similar result (not shown) has been found for integrated water content. The sensor design having forward and backward scans turns out to perform better than the sensor with single view for two CRM simulations, the Tropical squall line and the Mid-Atlantic cold front. On the other hand no improvement at all is found for the the Mid-Atlantic warm from simulation. For this simulation rain rates are typically lower than for the other two: the synthetic retrieval with only one viewing angle is already pretty good. Therefore rainfall retrieval improvements with fore/after viewing angles seem to be more relevant in high developed 3D structured clouds with high

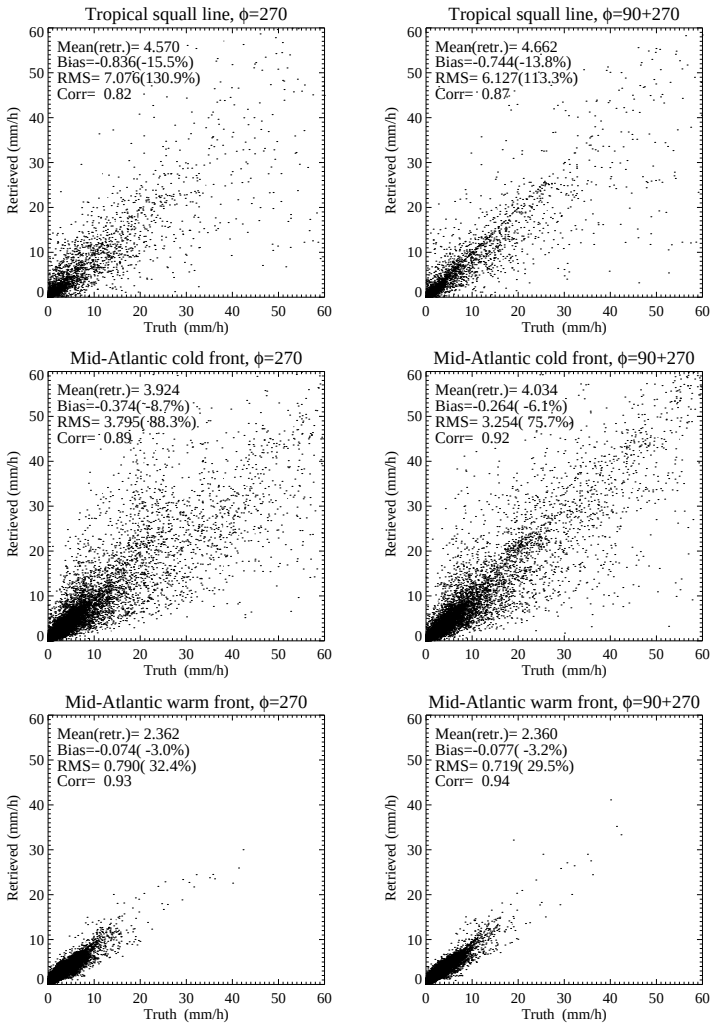

Figure 1.5. Scatter plot of true and retrieved rain rates from synthetic retrievals for the two radiometers ($\phi = 90$: forward and $\phi = 90 + 270$: forward and backward viewing) and the three CRM simulations.

rain rates. For these structures the presence of ice cores, uncorrelated with rainfall underneath, can mislead one viewing angle only radiometer, while in a less extent a fore/after viewing radiometer.

6. Conclusions

The fore/after view capability of new PMW sensors enhances the reliability of a 3D cloud observation, and as a consequence, improves

the retrievals of rain-rate and path integrated quantities and allows the identification of cloud features that, otherwise, can lead to errors in rain/no rain discrimination and rain estimation. To test the significance of the fore/after viewing angle concept, experimental data from air-borne radiometers with along track scanning radiometers and from space-borne radiometers with fore/after view (like Windsat) have to be analyzed and compared with independent observations. This will finally lead to applications in retrievals for drone GPM satellites and airborne high resolution scanning radiometers.

References

[1] Battaglia, A., and C. Kummerow, 2000: Forward Montecarlo computations of polarized microwave radiation, *Proceeding of 13th International Conference on Clouds and Precipitation*, Reno Area, Nevada, USA, pp. 256-259, 2000.

[2] Bauer, P., L. Schanz and L. Roberti, 1998: Correction of three dimensional effects for passive microwave remote sensing of convective clouds, *J. Appl. Meteor.*, **37**, 1619-1632.

[3] Goldhirsh, J., and B. Musiani, 1986: Rain cell size characteristics derived from radar observations at Wallops Island, Virginia. *IEEE. Trans. Geosci. Remote Sens.*, **GE-24**, 947-954.

[4] Haferman, J. L., Smith, T. F., and Krajewski, W. F., A multidimensional discrete ordinates method for polarized radiative transfer. I. Validation for randomly oriented axisymmetric particles, *J. Quant. Spectr. Radiat. Transfer*, **58**, 379-398, 1997.

[5] Hong, Y., J. L. Haferman, W.S. Olson and C. D. Kummerow, 2000: Microwave brightness temperatures from tilted convective systems, *J. Appl. Meteor.*, **39**, 983-998.

[6] Jorgensen, D. P., and M. A. LeMone, 1989: Vertical velocity characteristics of oceanic convection. *J. Atmos. Sci.*, **46**, 621-640.

[7] Kummerow, C., On the accuracy of the Eddington approximation for radiative transfer in the microwave frequencies, *J. of Geophysical Research*, **98**, 2757-2765, 1993.

[8] Kummerow, C., Beamfilling errors in passive microwave rainfall retrievals, *J. Appl. Meteor.*, **37**, 356-370, 1998.

[9] Liu, Q., Simmer, C., and Ruprecht E., Three-dimensional radiative transfer effects of clouds in the microwave spectral range *J. of Geophysical Research*, **101**, D2, 4289-4298, 1996.

[10] Platnick, S., Approximations for horizontal photon transport in cloud remote sensing problems, *J. Quant. Spectr. Radiat. Transfer*, 68, 75-99, 2001.

[11] Roberti, L., Haferman, J., and Kummerow, C., Microwave radiative transfer through horizontally inhomogeneous precipitating clouds, *J. of Geophysical Research*, **99**, 16, 707-716, 1994.

[12] Roberti, L., and Kummerow, C., Monte Carlo calculations of polarized microwave radiation emerging from cloud structures, *J. of Geophysical Research*, **104**, 2093-2104, 1999.

[13] Steiner, M., J. A. Smith, M. L. Baeck, Y. Zhang, and R. A. Houze, Jr., 2001: Space-time variability of heavy orographic rainfall. *Preprints, 30th International Conference on Radar Meteorology*, Munich, 19-24 July, American Meteorological Society, 527-529.

[14] Tao, W. K., and J. Simpson, 1993: Goddard cumulus ensemble model. Part I: Model description, *Terrest. Atmos. Oceanic Sci.*, **4**, 35-72.

[15] Shin, D. B., and C. D. Kummerow, Parametric rainfall algorithms for passive microwave radiometers, *J. Appl. Meteor.*, 2003.

[16] Weinman, J. A., and Davies, R., Thermal microwave radiances from horizontally finite clouds of hydrometeors, *J. of Geophysical Research*, **83**(6), 3099-3107, 1978.